CELLULAR ENERGY

Accelerating metabolism and transmembrane cation flux by distorting red blood cells

Philip W. Kuchel* and Dmitry Shishmarev†

Under static conditions, mammalian red blood cells (RBCs) require a continuous supply of energy, typically via glucose, to maintain their biconcave disc shape. Mechanical distortion, in a complementary way, should lead to increased energy demand that is manifest in accelerated glycolysis. The experimental challenge in observing this phenomenon was met by reversibly and reproducibly distorting the cells and noninvasively measuring glycolytic flux. This was done with a gel-distorting device that was coupled with ^{13}C nuclear magnetic resonance (NMR) spectroscopy. We measured [3-^{13}C]L-lactate production from [1,6-^{13}C]D-glucose in the RBCs suspended in gelatin gels, and up to 90% rate enhancements were recorded. Thus, for the first time, we present experiments that demonstrate the linkage of mechanical distortion to metabolic changes in whole mammalian cells. In seeking a mechanism for the linkage between shape and energy supply, we measured transmembrane cation flux with Cs^+ (as a K^+ congener) using ^{133}Cs NMR spectroscopy, and the cation flux was increased up to fivefold. The postulated mechanism for these notable (in terms of whole-body energy consumption) responses is stimulation of Ca–adenosine triphosphatase by increased transmembrane flux of Ca^{2+} via the channel protein Piezo1 and increased glycolysis because its flux is adenosine triphosphate demand–regulated.

INTRODUCTION

Cell shape and deformability

In the human cardiovascular circulation, each red blood cell (RBC; erythrocyte) traverses two narrow capillaries, on average, every 1 min; a typical capillary in peripheral tissues and the lungs has a diameter half that of the RBC. The capillary-imposed distortions that occupy ~1% of the blood circulation time, coupled with flow-induced shape changes, mean that RBCs spend a significant fraction of their ~120-day life span being dynamically distorted. Having an experimental means of quantifying biophysical and biochemical responses of RBCs to physical deformation (*1*) is fundamental to understanding their energy consumption (that is poorly characterized) and metabolic interactions with the vascular endothelium in tissues (*2*).

Even under static conditions, RBCs require a continuous supply of free energy via glycolysis (*3*) to maintain their biconcave disc shape (*4*). The deformability of the RBC depends on metabolism, with depletion of glucose promoting a morphological transition from discocyte to echinocyte and then spherocyte (*5*). The phenomenon of RBC "membrane flickering" that was first described in 1890 (*6*) has been vigorously investigated in recent years (*7*–*9*). The viscosity of the medium affects the frequency and amplitude of the membrane oscillations that suggests a metabolic driving force (*10*), but a less direct effect of energy supply acts via cytoskeletal (spectrin) rearrangements (*7*) that alter the phosphorylation state of an interconnecting protein, 4.1R, thus changing membrane-spectrin interactions (*11*). There is also some evidence that RBC deformation leads to adenosine triphosphate (ATP) release from the cells (*12*), although it is important to state that we found no evidence of this in the current work.

Mechanosensation in cells

Mechanosensory transduction via stretch-activated (mechanosensitive) ion channels links physical stimuli such as pressure and stretch to biological responses (*13*). Piezo1 and Piezo2 were the first mechanosensitive ion channels to be identified in mammalian cells (*14*–*16*), and their important role has been demonstrated in mechanical nociception (*17*) and vascular development (*18*).

Most investigations of the functions of the Piezo proteins have been carried out with electrophysiological patch clamping (*19*), but significant differences between outcomes of patch-clamping and whole-cell experiments have been mooted (*20*). Here, for the first time, we present experiments that demonstrate the linkage of mechanical distortion to metabolic changes in whole mammalian cells.

Metabolism-shape duality

Using this extensive background on effectors of RBC shape, deformability, and membrane flickering, we postulated that mechanically imposed distortion would increase energy utilization in RBCs, which is associated with an autonomous drive toward restoring their natural biconcave disc shape, and that it could be studied by NMR spectroscopy. If this reciprocal relationship existed (namely, shape maintenance requires energy delivered through metabolism, and reciprocally changing shape increases metabolic rate), it would pave the way to more quantitative experiments on factors that regulate shape and volume in all cells. We aimed to mechanically distort RBCs in a reproducible manner while noninvasively measuring their glycolytic flux.

Experimentally imposing shape changes

Variably stretchable gels have been previously used in analytical NMR spectroscopy to characterize mixtures of chiral compounds (*21*, *22*), to measure transmembrane exchange of deuterated water in RBCs (*23*) and to study the extent of ordering of cations inside RBCs (*24*). Recently, we demonstrated that RBCs are metabolically stable in carefully adjusted (with respect to pH and gelatin concentration) gels, and the cells become physically distorted in mechanically stretched/compressed gel samples (*25*). Here, we report the first-ever use of elastic gels to study the effects of mechanically induced shape changes on metabolic rate and cation transport in whole cells.

Aims and central hypothesis

We aimed to use the gels for holding RBCs in a distorted state, thus forcing their mechanosensitive ion channels (Piezo1) to stay open for

School of Life and Environmental Sciences, University of Sydney, Sydney, New South Wales, Australia.
*Corresponding author. Email: philip.kuchel@sydney.edu.au
†Present address: John Curtin School of Medical Research, Australian National University, Canberra, Australian Capital Territory, Australia.

influx of cations (Na^+, K^+, Cs^+, Mg^{2+}, Ba^{2+}, and Ca^{2+}) (*26*). Of these, Ca^{2+} carries the most significance, as the maximal velocity of Ca–adenosine triphosphatase (Ca-ATPase) (*27*) is more than twice that of Na,K-ATPase, which accounts for ~40% of the ATP turnover in the resting state of RBCs (*28*). Until now, this has been declared as "unused catalytic potential." We now postulate it to be part of the "rapid homeostatic response system" of the RBC, which is called upon under mechanical distortion during rapid flow in the bloodstream and in a more extreme manner in capillaries, as noted above.

RESULTS

RBC glycolysis in gels

The metabolic stability of human RBCs in elastic gelatin gels at 20°C is demonstrated in Fig. 1. ^{13}C NMR spectra were acquired from fresh cells suspended in pH-adjusted bovine gelatin gel to monitor conversion of [1,6-^{13}C]D-glucose (initially 9.95 mM) to [3-^{13}C]L-lactate. The ongoing glycolysis in the RBCs led to the decline of the glucose resonances (α and β anomers) at chemical shift, δ = 91.3 and 95.1 parts per million (ppm), respectively, and the emergence of the resonances of [3-^{13}C]2,3-bisphosphoglycerate (23BPG) and [3-^{13}C]L-lactate at δ = 65.6 and 19.3 ppm, respectively. The resonance at δ = 13.1 ppm was from [6-^{13}C]L-methionine that had been added as an internal peak integral standard; it remained of the same intensity throughout the 45-hour time course. These data showed that the RBCs remained metabolically active for at least 45 hours in the gel, generating [3-^{13}C]L-lactate at a constant rate (see fig. S1 for the graph and the measured rate of glycolysis).

Stretching the silicone rubber tube to 1.7 times its original length, while the RBC-gelatin sample was still in the liquid state, and then allowing the gel to form at 10°C yielded a sample in which the RBCs were described as "70% compressed" when the tension in the silicone tube was released. When the RBC-gelatin sample was allowed to gel at 10°C in a relaxed silicone tube, it could be stretched to various extents up to twice the original length before the gel broke.

Seventy percent compression routinely yielded significant glycolytic rate enhancements like that shown in Fig. 2; however, stretching the sample by 70% always gave smaller enhancements (~60% of the corresponding compression value). We postulate that this is due to the fundamental difference in the anisotropy of the strain field in the gel imposed by stretching and compression.

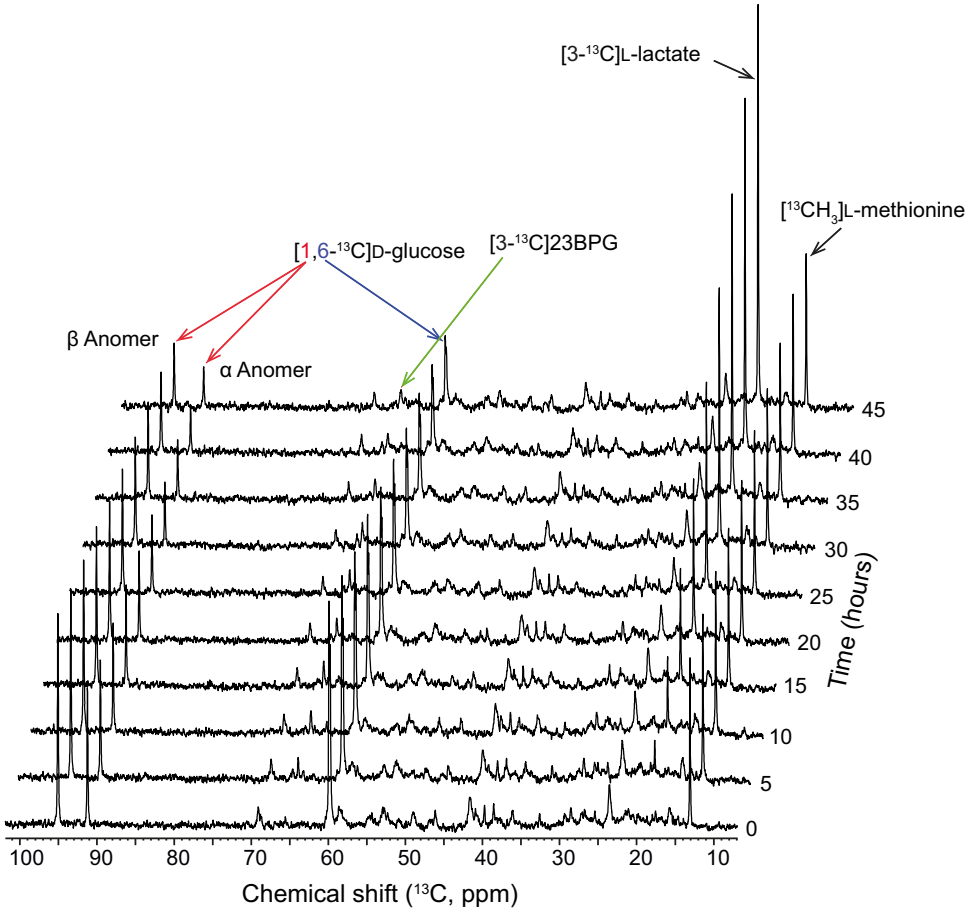

Fig. 1. ^{13}C NMR (100.61 MHz) spectral time course of human RBCs metabolizing [1,6-^{13}C]D-glucose in relaxed gelatin gel. Suspension medium was 60 mM NaOH, 110 mM NaCl, 10 mM KCl, and 10 mM $CaCl_2$ at pH 7.4 and 20°C with 9.95 mM [1,6-^{13}C]D-glucose. Resonance assignments were as follows: 91.3 and 95.1 ppm, C1 of α and β anomers of [1,6-^{13}C]D-glucose; 65.6 ppm, C3 of 23BPG; 59.8 ppm, partially resolved C6 of α and β anomers of [1,6-^{13}C]D-glucose; 19.3 ppm, methyl carbon of [3-^{13}C]L-lactate; 13.1 ppm, methyl carbon of [6-^{13}C]L-methionine added as an intensity reference; and 0 ppm, natural-abundance ^{13}C in a silicone rubber tube used as the chemical-shift reference. A ~30° excitation pulse was used, with a recovery delay of 2 s per free induction decay (FID), to acquire 816 transients per spectrum, giving a total acquisition time of 30 min. For clarity, only every 10th spectrum is shown.

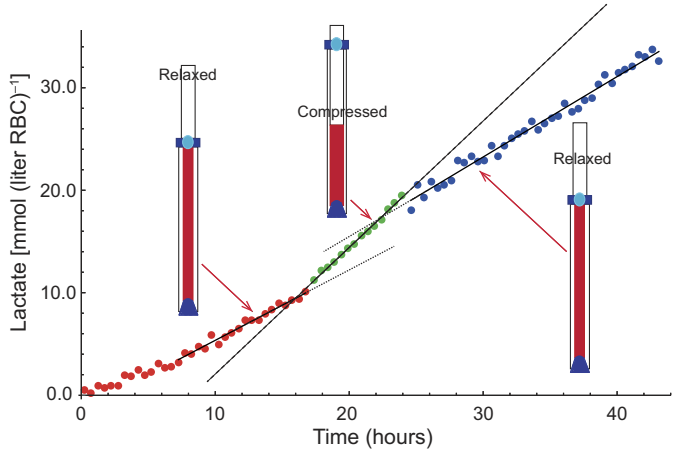

Fig. 2. Reversible effect of mechanical deformation of RBCs on their glycolytic rate. [3-^{13}C]L-Lactate production by RBCs in gelatin gel at 20°C was recorded from 9.95 mM [1,6-^{13}C]D-glucose in the same suspension medium, as for Fig. 1. As shown by the insets, the RBC/sample was initially relaxed (red circles), then 70% compressed (green circles), and relaxed again (blue circles). The amount of produced [3-^{13}C]L-lactate was calculated from the peak integrals of its methyl resonance, relative to that of standard [$^{13}CH_3$]L-methionine, in the sequential ^{13}C NMR spectra. For each spectrum, 812 transients were acquired for a total time of 30 min using a ~30° excitation pulse with a duration of 17.5 μs and an intertransient delay of 2 s. Before Fourier transformation, a decaying exponential window function with a line-broadening factor of 5 Hz was applied. The data were imported into a program written in Mathematica (*49*) that automatically performed spectral peak fitting, thus allowing us to calculate peak integrals. Calculation of the [3-^{13}C]L-lactate concentration was performed by calibration of the peak integrals relative to the standard compound ([$^{13}CH_3$]L-methionine present at a concentration of 5.32 mM). The solid lines are least-squares regression fits to the data, and the dashed lines are extrapolations that emphasize the major change in slope that reversibly occurred on transitioning between the stages (see text). Two-tailed Student's *t* tests indicated no statistically significant difference at $P < 0.05$ for the first and second relaxed-state slopes, and significant difference at $P < 0.01$ with respect to the middle slope.

Canonical experiment

Figure 2 shows a time course of [3-^{13}C]L-lactate production (sample prepared and measured in a manner similar to that for Fig. 1) that initially had RBC/gel in a relaxed state, then the sample was 70% compressed, followed by returning it to the original relaxed state. As seen in the time course, there was an initial transient stage in the production of [3-^{13}C]L-lactate. This was the result of washout of unlabeled metabolites into lactate, especially from 23BPG, but after ~8 hours, this stabilized to a constant rate of 0.67 ± 0.02 mmol (liter RBC)$^{-1}$ hour^{-1}. In the subsequent compressed state, the rate markedly increased to 1.23 ± 0.02 mmol (liter RBC)$^{-1}$ hour^{-1} (~80% enhancement of the glycolytic rate in this case), and after returning to the relaxed state, the rate dropped to a value similar to the initial one, viz, 0.80 ± 0.01 mmol (liter RBC)$^{-1}$ hour^{-1}.

The marked enhancement of the glycolytic rate in the compressed sample (Fig. 2) had a significant dependence on the presence of Ca^{2+} in the suspension medium. When the ^{13}C NMR time-course experiments in Fig. 2 were carried out in the absence of Ca^{2+}, the extent of enhancement of glycolysis during RBC compression was invariably less than 10% of that in the relaxed state. Glycolytic rate enhancement was saturable with respect to Ca^{2+} concentration, with 10 mM giving the maximum extent that we observed (~80%), whereas 2 mM Ca^{2+} gave a value of ~50%.

Membrane transport in gels—^{133}Cs NMR

Having established that distortion-enhanced metabolism was dependent on Ca^{2+}, we postulated that the effect was mediated by Piezo1 (*29*). Therefore, we tested whether the transmembrane cation fluxes in whole RBCs would also be sensitive to cell distortion. Figure 3 shows the reversible enhancement of $^{133}Cs^+$ efflux from Cs^+-loaded RBCs when they were compressed in a gel, prepared in the same manner as for Figs. 1 and 2 (and fig. S1). The RBCs had been preloaded with $^{133}Cs^+$ by incubating them for 2 days at 21°C in isotonic NaCl-saline, in which 100 mM CsCl replaced the equivalent NaCl. Extracellular $^{133}Cs^+$ was removed by two cycles of centrifugation upon resuspending the cells in 154 mM NaCl. At the start of the time course in Fig. 3, the ^{133}Cs NMR spectrum showed a single prominent resonance at δ = 11.6 ppm, corresponding to the $^{133}Cs^+$ inside the cells. Over the course of 2 hours, there was growth of a second peak, corresponding to extracellular $^{133}Cs^+$. The lower inset in Fig. 3 shows the third spectrum acquired with a substantial extracellular resonance at δ = 10.55 ppm.

After 2 hours, the tension in the silicone tube was released to compress the gel, and recording $^{133}Cs^+$ efflux continued for the next 2 hours. Regression of a straight line onto the data at this stage showed that the rate of efflux had increased 5.4-fold (Fig. 3).

Quantifying the extracellular peak integral required special analysis because $^{133}Cs^+$ in the anisotropic environment of the stretched gelatin gel displays quadrupolar splitting (*24*). A singlet in relaxed gel became a septet (^{133}Cs has a nuclear spin of 7/2) on compression or stretching due to spatial anisotropy of the gel, causing residual quadrupolar coupling (see Supplementary Discussion) (*30*).

In the third stage of the experiment, the silicone tube was stretched to 1.7 times its previous length, thus returning the contents back to the relaxed state. ^{133}Cs NMR spectra showed a gradual rise of the resonance from the extracellular $^{133}Cs^+$. The slope of the line regressed from these data was substantially smaller than that in the first stage, because the system was approaching equilibrium.

The $^{133}Cs^+$ efflux experiment in Fig. 3 followed the same sequence of relaxed-compressed-relaxed as the metabolic one in Fig. 1, but the cation flux had a much greater rate enhancement (a factor of >5). The results of a complementary experiment with the sequence of stages in the reverse order in Fig. 3 are shown in fig. S2.

Glycolysis in RBC suspensions

Apart from mechanical stimuli, Piezo1 is activated chemically by the compound yoda1, which is known to enhance transmembrane Ca^{2+} flux (*31*). ^{13}C NMR spectra of RBC suspensions without and with added yoda1 are shown in Fig. 4, and they display the same resonances as in Fig. 1. Because the RBC suspensions (not in gel) were incubated at 37°C, the rate of lactate production was much higher, with a 50% extent of reaction after ~4 hours. When 2 μl of 28.15 mM yoda1 [dissolved in dimethyl sulfoxide (DMSO)], giving a final concentration of 19 μmol (liter sample)$^{-1}$, was added to an identical sample, the time course in Fig. 4B was obtained. Note the marked enhancement of lactate production over the control experiment (Fig. 4A).

Experiments carried out with differences in suspension medium, and with either [2-^{13}C]acetate or [6-^{13}C]L-methionine as intensity references, revealed that specific intensities of the signals from the various metabolites differed between experiments. Therefore, control rates were scaled to one value, 3.00 mmol (liter RBC)$^{-1}$ hour^{-1}, as reported in our previous studies of human RBC metabolism (*32*). The rates of lactate production in the two time courses (Fig. 4) were 3.0 ± 0.5 mmol (liter

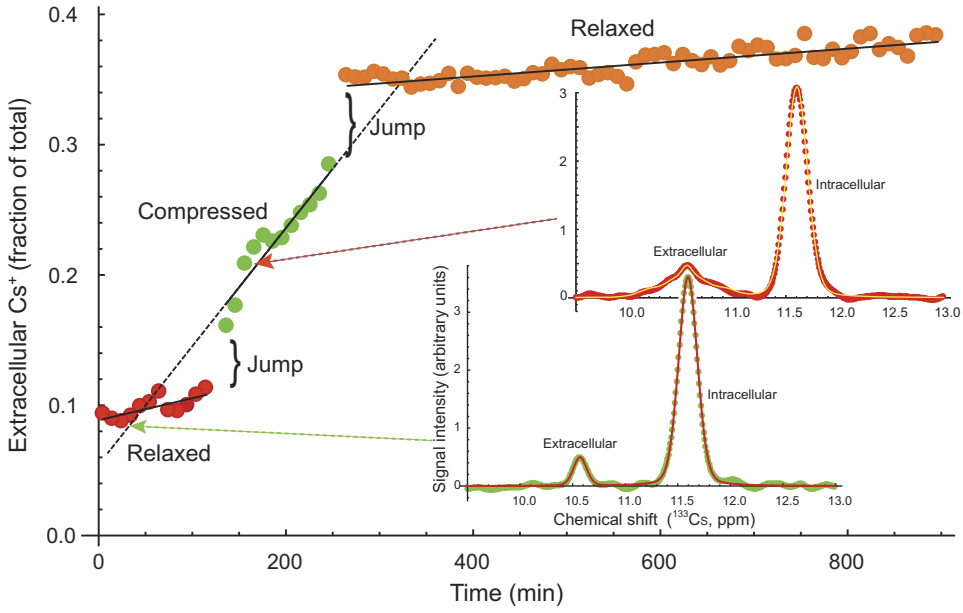

Fig. 3. Reversible effect of compression on efflux of Cs^+ from human RBCs. Cs^+-loaded RBCs were suspended in gelatin gel that was relaxed (red circles), 70% compressed (green circles), and then relaxed again (orange circles). Net $^{133}Cs^+$ efflux was measured with ^{133}Cs NMR (52.48 MHz) spectroscopy at 20°C by recording 12 sequential spectra in each stage. The sample was from the same batch of RBCs used for fig. S2 and treated in the same manner. Fitted slopes obtained with NonlinearModelFit in Mathematica, for the respective stages, were $(1.7 \pm 0.5) \times 10^{-4}$ min^{-1} $(9.1 \pm 0.9) \times 10^{-4}$ min^{-1} and $(0.53 \pm 0.04) \times 10^{-4}$ min^{-1}. With an initial intracellular $[Cs^+]$ of 16.5 mM, these rates corresponded to respective effluxes of 2.8 ± 0.8 μmol (liter RBC)$^{-1}$ min^{-1}, 15.0 ± 1.5 μmol (liter RBC)$^{-1}$ min^{-1}, and 0.80 ± 0.07 μmol (liter RBC)$^{-1}$ min^{-1} (where "±" denotes SE, and the second-stage rate is significantly different from the first at $P < 0.05$). The two inset spectra correspond to the third point in the respective time course, where the dots are the data points and the solid line is a least-squares fit of a line-shape function (described in Materials and Methods) to the spectra, performed with NonlinearModelFit in Mathematica. Note that the chemical shift scale runs from left to right according to the mathematical convention used in Mathematica, but this is opposite to the convention in NMR spectroscopy. The apparent "jumps" in flux that arose at the beginning and end of the compression stage were an artifact of the broad baseline in the compressed gel (see the Supplementary Materials under "$^{133}Cs^+$ efflux from RBCs in gels" for further comment).

RBC)$^{-1}$ hour^{-1} and 6.9 ± 0.3 mmol (liter RBC)$^{-1}$ hour^{-1}, indicating a 2.3-fold enhancement brought about by yoda1.

Cesium chloride (30 mM) was included in the NaCl-saline medium because it was used in other experiments that are listed in table S1. It affected the net rate of glycolysis relative to a medium in which sucrose replaced NaCl as the main osmotic support. To explore these differences further, and to probe the action of known effectors of cation transport in human RBCs, the following experiments were carried out, with the results summarized in table S1.

In NaCl-saline medium, yoda1 stimulated the rate of RBC lactate production by a factor of ~3, an effect replicated in three experiments but not in a fourth (table S1; row 1 compared with row 2, 9 with 10, 17 with 18, and 37 with 38). In addition, in separate experiments, we added eosin, *p*-chloromercuribenzenesulfonate (*p*CMBS), ammoniated ruthenium oxychloride (ruthenium red), calmidazolium, and peptide GsMTx4 (*38*).

Eosin is a Ca-ATPase inhibitor in RBCs (*33*), but even at the high concentration of 150 μM, it had no effect on the yoda1-stimulated glycolytic rate, whereas *p*CMBS reacts with exposed sulfhydryl groups in proteins, including the integral membrane water transporter, aquaporin 1, in RBCs (*34*). Even at the high concentration of 150 μM, eosin had no effect on the yoda1-stimulated glycolytic rate, whereas *p*CMBS diminished the yoda1-enhanced response to around two-thirds of the control value, implying that exposed –SH groups are involved with the binding of the compound to Piezo1 or to a protein in close juxtaposition in the membrane.

Ruthenium red is an inorganic dye that interacts with many proteins, including being an inhibitor of mitochondrial Ca^{2+} transport (*35*), and the transient receptor potential (TRP) ion channel (*36*) that has electrophysiological characteristics similar to those of Piezo1. At concentrations of 240 and 400 μM, it had no significant effect on yoda1-induced stimulation of glycolysis.

Calmidazolium binds to calmodulin and inhibits Ca-ATPase in nerve cells (*37*). With RBCs in NaCl-saline, it stimulated glycolysis by ~80% (table S1; row 15 versus row 9). Additionally, in the presence of yoda1, the previously attained ~3-fold enhancement was reduced to 2.4-fold (row 16/row 9). This provided further evidence of (at least indirect) involvement of Ca^{2+} in the yoda1-stimulated metabolic response.

^{133}Cs NMR spectra of RBCs with $^{133}Cs^+$ in the extracellular medium showed immediate cation influx after the addition of 19 μM yoda1. Of great relevance was the inhibition of yoda1-initiated $^{133}Cs^+$ influx (lower curve in fig. S3B) by GsMTx4. This peptide toxin is a known inhibitor of Piezo1 (*38*, *39*), so this result provided solid evidence of a Piezo1-mediated mechanism of the observed $^{133}Cs^+$ transport.

DISCUSSION

Various aspects of the experimental design and data analysis are discussed in detail in Supplementary Discussion. Here, we focus on the overall, more general interpretation of the results.

Model of RBC shape distortion responses

Figure 5 shows a schematic diagram of the biochemical systems we postulate to be involved in the compression/stretched-induced glycolytic and $^{133}Cs^+$ flux responses that were observed. The caption lists the transporters, pumps, and overall glycolytic metabolism that are interconnected in the responses.

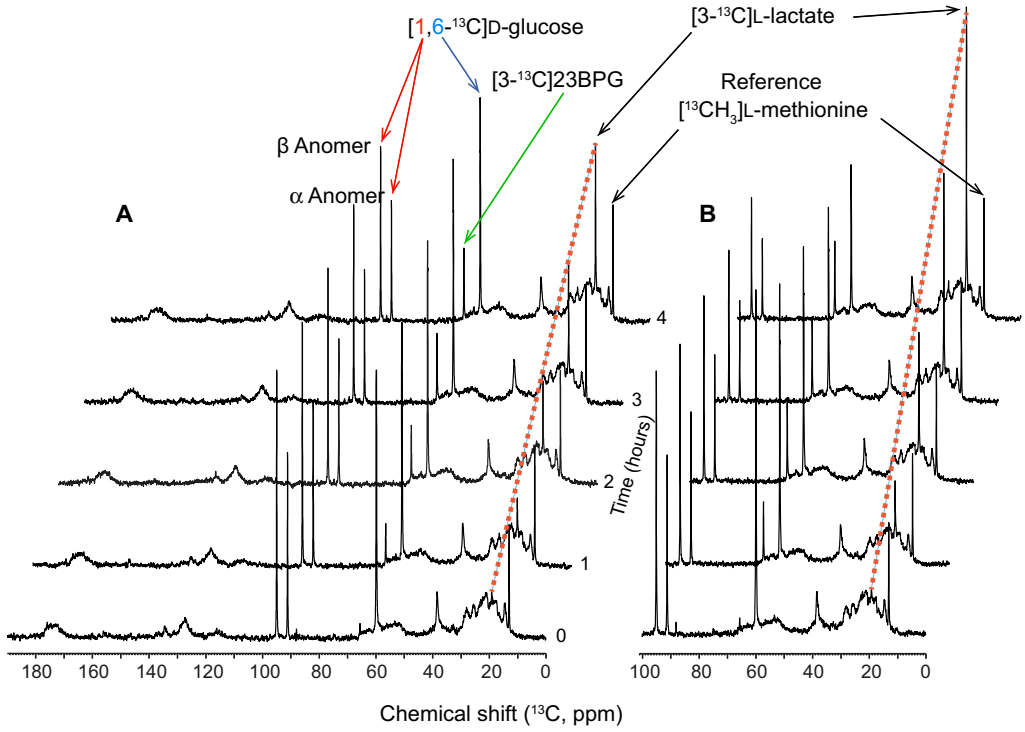

Fig. 4. Stimulation of glycolysis by yoda1. ^{13}C NMR (100.61 MHz) spectra of human RBCs metabolizing [1,6-^{13}C]D-glucose in a gel-free suspension at 37°C and hematocrit (Ht) = 75%, (**A**) without and (**B**) with yoda1. For each spectrum, 176 transients of 8192 data points were acquired in 6.87 min using a ~30° excitation pulse of 17 μs and an intertransient delay of 2 s. Before Fourier transformation, a decaying exponential window function with a line-broadening factor of 8 Hz was applied. The RBC suspension medium was as follows: 30 mM CsCl, 10 mM KCl, and 114 mM NaCl, with an osmolality of 282 mosmol kg^{-1}; 8.2 mmol (liter sample)$^{-1}$ or 10.39 mmol (liter aqueous space)$^{-1}$ [1,6-^{13}C]D-glucose; 5.13 mmol (liter sample)$^{-1}$ or 4.05 mmol (liter aqueous space)$^{-1}$ [6-^{13}C]L-methionine; 2.1 μl of 1 M stock, giving 0.88 mmol (liter aqueous space)$^{-1}$ or 2.8 mmol (liter extracellular aqueous space)$^{-1}$ [Ca^{2+}]; and 2.0 μl of 28.15 mM stock in DMSO, giving 19 μmol (liter sample)$^{-1}$ yoda1. Because the mean RBC volume was 86 fl, there were 2.61 × 10^{10} cells in the sample, implying 4.4 × 10^{8} yoda1 molecules per cell.

Compression-induced glycolytic enhancement is explained by the opening of Piezo1 with the consequent influx of Ca^{2+}, stimulating Ca-ATPase. This enzyme/pump reduces the concentration of ATP that, in turn, reduces the high-substrate inhibition of hexokinase, at its allosteric site, and accelerates glycolysis (*32*, *40*–*42*).

Because the RBCs are held in a distorted state, Piezo1 stays open (on average) and is subject to "usage activation" (*26*), a phenomenon observed after repeated stimulation in patch-clamping experiments. The high maximal velocity of RBC Ca-ATPase (*43*), which is more than twice that of Na,K-ATPase that accounts for ~40% of the ATP turnover in normal resting RBCs (*28*), has been an enigma. It had been surmised that the high V_{max} of Ca-ATPase represented unused catalytic potential. However, we now postulate that this high catalytic capacity is exploited most extensively during the ~700 ms every minute when RBCs are distorted in capillaries during normal blood flow. It is part of the rapid homeostatic response system of the RBC.

We hypothesize that, once elevated at the site of entry through Piezo1, the Ca^{2+} signals locally to the cytoskeleton to bring about structural rearrangements that lead to strain in the protein network, which drives a return of the cell to its original biconcave shape. The duration of this signal (of cell distortion) is determined by the rapid ejection rate of Ca^{2+} from the RBC by Ca-ATPase.

Future directions

The role of the cytoskeleton in the metabolic and cation transport responses warrants further investigation. Changes in the arrangement of spectrin could be contributing to what is called mechanoprotection (*26*) that reduces the extent of the effects we report here. The metabolic and cation transport effects we observed were rapidly reversible (Figs. 2 and 3 and fig. S2), so this points to membrane-protein shape changes as the trigger. This is not a covalent modification or phosphorylation but simply mechanical distortion of Piezo1. Following downstream in this signaling cascade is rearrangement of the cytoskeleton on a longer time scale (minutes) based on protein phosphorylation affecting overall deformability (*7*, *11*).

The participation of endogenous effector ligands in the reported metabolic and cation transport responses has not yet been explored/discovered. However, in view of the recent finding of lactate gating of carotid body glomus cell Ca^{2+} flux (*44*), this is an area worth investigating in RBCs.

CONCLUSIONS

It is a fundamental property of all cells that they sense mechanically and physicochemically induced changes in their shape. We report here a new noninvasive approach to quantifying perturbations of cellular metabolism and transmembrane cation flux that are brought about by altering the shape of cells. This was done by first suspending the cells in a gel and then mechanically distorting the whole sample. Another challenge when developing this study was to inspect inside the cells and record changes in their metabolite composition and transmembrane cation distributions. This was achieved using NMR spectroscopy with its

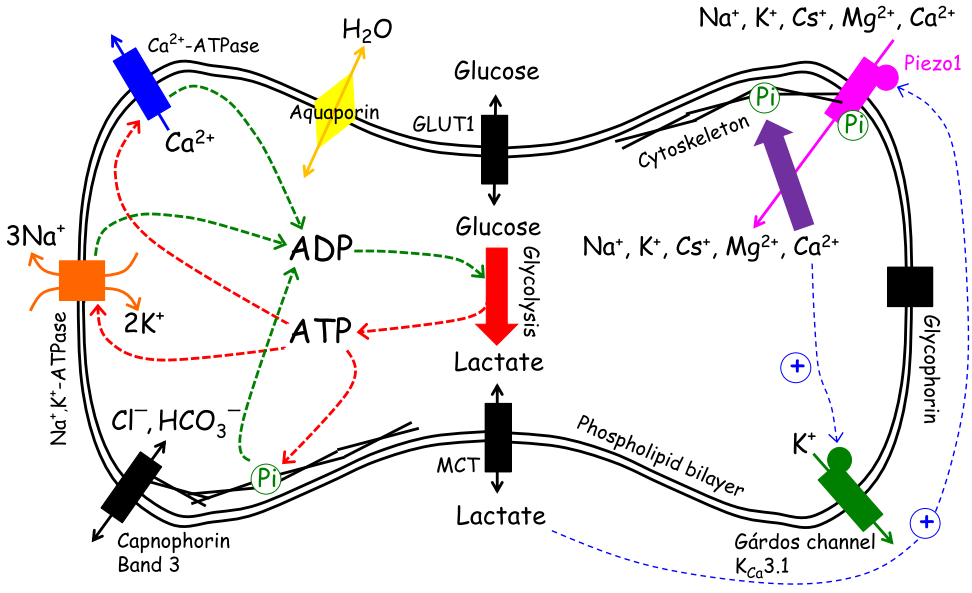

Fig. 5. Schematic representation of the Ca^{2+}-mediated linkage between activation of Piezo1 by mechanical distortion of the RBC and stimulation of its glycolysis. The various participants in this complex response are as follows: GLUT1, which is the glucose transporter required to deliver this fuel molecule to the cytoplasm; Ca-ATPase, which responds to an increase in [Ca^{2+}] by catalyzing the hydrolysis of one molecule of ATP per Ca^{2+} ion ejected from the cytoplasm; and Na,K-ATPase, which constitutively pumps three Na^+ ions from the cell while simultaneously importing two K^+ ions with the concomitant hydrolysis of one molecule of ATP; in the physiological operation of the RBC, this reaction consumes ~40% of the free energy derived from glycolysis (*28*, *32*). Capnophorin (also called Band 3) catalyzes the one-for-one exchange of the anions, Cl^- and HCO_3^-, and is central to the attainment of bulk electroneutrality. The monocarboxylate transporter (MCT) mediates the facilitated diffusion of lactate across the RBC membrane. Its operation was evident from the splitting of the [3-^{13}C]L-lactate resonance that indicated two compartments (inside and outside the RBCs) from the ^{13}C NMR spectral time courses. The Gárdos channel (also called $KCa_{3.1}$ or KCNN4) mediates the efflux of K^+ under the control of Ca^{2+}. The membrane protein glycophorin is linked to the cytoskeleton, as is capnophorin; these linkages are made in as yet to be defined ways, but they are affected by Ca^{2+}. Piezo1 mediates the exchange of both monovalent and divalent cations, with permeabilities (*P*) in the order of $P_{K+} > P_{Na+} \approx P_{Cs+} > P_{Li+} \gg P_{Ca2+}$ (*26*). The free energy of covalent bond cleavage of glucose and its subsequent metabolites is captured as anhydride bond energy in ATP. This "energy currency" molecule is "spent" on driving the two ATPases shown in the diagram, as well as other kinase reactions not shown, producing adenosine diphosphate (ADP). Glycolysis is ATP demand–regulated so increased influx of Ca^{2+} stimulates Ca-ATPase that increases ATP hydrolysis and hence glycolytic flux. The positive feedback of extracellular lactate to Piezo1 is only speculated to occur in RBCs based on the findings on glomus cells from the carotid body (*44*).

almost unique capability to record signals from ions and metabolites in cells.

Drugs affecting the pathways involved in the connection between cell shapes and metabolism will potentially lead to the ability to manipulate biochemical and energetic steady states in the whole body. The experimental approaches described here are ready for application to other more phylogenetically primitive cells and to highly evolved ones, including those in pathological states like neoplasia.

MATERIALS AND METHODS

Chemicals and solutions

Analytical reagent chemicals were purchased from Sigma-Aldrich, unless otherwise indicated. The saline used for the preparation of all RBC samples (154 mM NaCl) was filtered three times through a 0.2-μm membrane filter (Millipore) to remove potentially infective particulate matter. The osmolality of each solution was adjusted to 290 ± 5 mosmol kg^{-1} guided by a vapor pressure osmometer (model 5520, Wescor Instruments).

Red blood cells

Blood was obtained by venipuncture from the cubital fossa of consenting healthy donors under the approval of the University of Sydney Human Ethics Committee (Institutional Review Board) for the project. Heparin (15 U ml^{-1}) was added as the anticoagulant, and the blood was centrifuged at 3000*g* for 5 min at 4°C. The plasma and buffy coat were removed by vacuum pump aspiration. The RBC pellet was washed three times in five volumes of saline, with repeated centrifugation and supernatant aspiration. Before the last wash, the RBC suspension was bubbled with carbon monoxide for 10 min to convert the Fe(II) in hemoglobin to its stable diamagnetic form in carboxyhemoglobin. For prolonged time courses, the final washing medium contained penicillin G and streptomycin (both 75 μM) to prevent bacterial growth. The Ht, measured using a capillary centrifuge (12,000*g*; Hermle, Z252M), was typically 0.85. The samples were stored at 4°C for up to 24 hours until use.

Gels

Gelatin (1.75 g, grade 20N, Gelita) was dissolved in 5 ml of "neutralizing saline" consisting of 60 mM NaOH, 110 mM NaCl, and 10 mM KCl. This particular amount of NaOH yielded pH 7.4 in the otherwise acidic gelatin solution. The mixture was heated for ~20 min at 60°C in a water bath until dissolution occurred and then was cleared of air bubbles by centrifugation at 2000*g* for 30 s.

RBC suspension (2.0 ml, Ht ~ 0.85) was added to the gelatin solution at 42.0°C to give a final Ht ~ 0.20. The sample was gently mixed (so as not to introduce new bubbles) with a spatula, withdrawn into a silicone rubber tube of 5.0-mm inside diameter (ID) and 6.9-mm outside diameter (OD) (Sims Portex) with a 5-ml disposable syringe, and sealed with a Delrin plug. The time of exposure of the RBCs to higher than physiological temperatures was kept to ~2 min to avoid

potential metabolic and/or morphological changes. The samples were inserted into bottomless thick-walled glass NMR tubes of 8.0-mm ID and 10.0-mm OD (New Era Enterprises) and then stored at 10°C for ~30 min to promote gelation. Stretching the gels was achieved in the previously described apparatus (further information about the apparatus is given in the Supplementary Materials) (*21*, *45*). For gels destined for later compression, the silicone rubber tube was stretched inside the outer glass tube while the gelatin was still in the liquid state. After gelation, the sample was compressed by releasing the thumbscrew. The "extent of stretching" or compressing the gels (and RBCs), ε, was defined as

$$\varepsilon = \frac{|l - l_0|}{l_0} \times 100\% \quad (1)$$

where l is the length of the elastic tube in the stretched/compressed state and l_0 is the original length of the elastic tube up to the rim of the outer glass tube.

Samples used for ^{13}C NMR measurements were prepared as described previously (*25*), with the addition of 9 to 15 mM [1,6-^{13}C]D-glucose; they were incubated for up to 45 hours in either relaxed or stretched states (ε = 50 to 70%) at 20°C.

Calculation of solute and ion concentrations in RBC-gelatin samples

Because the gelatin concentration used in making the RBC suspensions (350 g liter^{-1}, w/v; see additional comment on this below) was comparable to that of the hemoglobin inside the cells, we calculated concentrations of ions and solutes on a per-aqueous volume basis as follows.

1) In a sample prepared as described above, 1.75 g of gelatin was dissolved in 5 ml of neutralizing saline. The partial specific volume of gelatin, $\bar{v}$ = 0.7417 ml g^{-1} (*46*), implied that its volume was 1.75 × 0.7417 = 1.3 ml. This, coupled with the volume of neutralizing buffer (5 ml) and RBC suspension (2.0 ml), inferred a total sample volume of 8.3 ml. Two milliliters of this preparation was drawn into each silicone rubber tube and sealed at the bottom with a Delrin plug.

2) In 2 ml of RBC suspension of Ht = 0.865, the aqueous volume is made up of the water in the extracellular space, viz, 2.0 × (1 − Ht) = 0.27 ml, and the water inside the cells. The latter was calculated as 2.0 × Ht × α = 1.24 ml, where α = 0.717 is the volume fraction, of an isovolumic human RBC, that is occupied by water (*47*).

3) The volume of neutralizing saline was 5.0 ml, so the total extracellular aqueous volume was 5.0 + 0.27 = 5.27 ml. The total water in the sample in both compartments was therefore 5.0 + 0.27 + 1.24 = 6.51 ml.

4) To make the Ca^{2+} concentration of 10 mM in the extracellular space at the start of an experiment, the volume of added 1 M $CaCl_2$ was 53 μl.

5) With [1,6-^{13}C]D-glucose and [6-$^{13}CH_3$]L-methionine, the amounts added were chosen to give concentrations as if they were averaged over the total aqueous volume of the sample. For example, for the sample used to generate Fig. 1, 11.86 mg of [1,6-^{13}C]D-glucose yielded a concentration of 9.95 mM in the aqueous space, whereas 5.2 mg of [$^{13}CH_3$]L-methionine gave a concentration of 5.32 mM.

6) The effective Ht across the whole sample volume was 2.0 × Ht = 0.865/8.3 = 0.208. Therefore, when the amount of [1-^{13}C]L-lactate was computed during a spectral time course, based on relativity with the peak integral of the known concentration of [6-$^{13}CH_3$]L-methionine, it was rescaled to give the rate per liter of whole RBCs by dividing by 0.208 (for example, as for Fig. 2).

Calculation of $^{133}Cs^+$ concentrations in RBC-gelatin samples

The rationale for estimating the concentration of $^{133}Cs^+$ inside the RBCs in a compressed gel experiment was as follows (using the particular numerical values associated with the samples used for Fig. 3 and fig. S2).

1) A typical $^{133}Cs^+$ loading protocol involved suspending 15 ml of saline-washed RBCs (called the RBC sample volume below) of Ht_1 = 0.8 (subscript 1 denotes the first Ht measured) in 35 ml (denoted below as "Cs saline volume") of Cs^+-saline: 100 mM CsCl, 44 mM NaCl, 5 mM K_2HPO_4, 15 mM D-glucose, 10 mM inosine, 0.075 mM penicillin G, and 0.075 mM streptomycin. This gave a total water volume in the incubated sample of 0.8 (Ht_1) × 0.717 [this is the α value or aqueous volume fraction of RBCs (*47*)] × 15 ml ("RBC sample volume") + 35 ml (Cs saline volume) = 43.6 ml and Ht_2 = 0.24 (subscript 2 denotes the second Ht value).

2) At the start of the incubation, the $^{133}Cs^+$ concentration outside the RBCs was 100 mM (denoted below as $[Cs^+]^{start}$), and yet, if it was averaged over the whole aqueous volume, it was 30.0 × 100.0/43.6 = 68.8 mM. After incubation for 4 days at 4°C, or for 2 to 3 days at 21°C with one change of incubation medium, the sample was centrifuged (3000*g* for 5 min at 10°C) and the pellet, plus some residual supernatant, gave the final Ht_3 = 0.785 (subscript 3 denotes the third Ht value). A ^{133}Cs NMR spectrum was recorded from 3 ml of this suspension: In the particular example discussed here, it gave relative peak integrals of intracellular/extracellular = 0.41:0.59.

3) At the final "steady state," the concentration of $^{133}Cs^+$ inside the cells, $[Cs_i^+]^{ss}$, was related to the concentration in the extracellular space, $[Cs_e^+]^{ss}$, through the relative signal intensities $Sig_i/Sig_e = Sig_r$ and the relative compartment volumes $(1 - Ht_3)/Ht_3$. Thus,

$$[Cs_i^+]^{ss} = \frac{Sig_r(1 - Ht_3)}{Ht_3}[Cs_e^+]^{ss} \quad (2)$$

4) The conservation of mass condition for total $^{133}Cs^+$ in the incubation suspension was

$$\begin{aligned} &Ht_1 \times \text{RBC sample volume} \times [Cs_i^+]^{ss} + ((1 - Ht_1) \times \\ &\text{RBC sample volume} + \text{Cs saline volume})\ [Cs_e^+]^{ss} \\ &= \text{original number of moles of } ^{133}Cs^+ (\text{viz, } 30 \text{ ml} \\ &\times 100 \text{ mM} = 0.003 \text{ mol}) \end{aligned} \quad (3)$$

5) Rearranging Eq. 3 to obtain an expression for $[Cs_i^+]^{ss}$ in terms of the other parameters and the initial concentration, $[Cs^+]^{start}$, we obtained

$$[Cs_i^+]^{ss} = \frac{\text{Cs saline volume} \times [Cs^+]^{start}(1 - Ht_3)\, Sig_r}{\text{Cs saline volume}\, Ht_3 + \text{RBC sample volume}\,(Ht_1(Sig_r - Ht_3\,(1 + Sig_r)) + Ht_3)}$$

and then using the numerical values stated above

$$[Cs_i^+]^{ss} = \frac{0.035 \times 0.1 \times (1–0.785) \times \left(\frac{0.41}{0.59}\right)}{0.035 \times 0.785 + 0.015 \times \left(0.80\left(\frac{0.41}{0.59}\right) - 0.785\left(1 + \frac{0.41}{0.59}\right) + 0.785\right)}$$

$$= 16.5 \text{ mmol (liter RBC)}^{-1} \quad (4)$$

Solving for $[Cs_e^+]^{ss}$ gives its concentration as 86.9 mmol [liter extracellular solution]$^{-1}$.

6) RBCs with this concentration of Cs^+ were centrifugally washed twice (as described above) in four volumes of 154 mM NaCl containing 15 mM D-glucose, thus removing Cs^+ from the extracellular medium. Four milliliters of these RBCs (Ht = 0.86) was added to the gelatin solution, as described in the "Gels" section, at 42°C, giving a final Ht of 0.2.

Calculation of [3-^{13}C]L-lactate concentrations in RBC suspensions

1) Use of calibration standards: Known amounts of [1,6-^{13}C]D-glucose were added to RBC suspensions to measure the rate of glycolysis in the absence and presence of yoda1. To calibrate the resonance intensities of glucose and lactate to their concentrations, and hence calculate the glycolytic rate, a known amount of [6-^{13}C]L-methionine was added to the sample as the peak intensity reference; its chemical shift was δ = 13.1 ppm. However, to improve the signal-to-noise (S/N) ratio in the NMR spectra, a rapid repetition rate of radio frequency (RF) pulses was used. This led to a steady state of partial saturation of the magnetization of the various spin populations in the sample, and these differed between the solute species. Thus, integrals (and amplitudes) of different peaks from molecules at the same concentration had different values. The following analysis was used to calibrate the methyl resonance intensity of [3-^{13}C]L-lactate to its underlying concentration.

A known amount of pure [3-^{13}C]L-lactate was added to a sample of RBCs in a suspension, or a known amount of [1,6-^{13}C]D-glucose was allowed to be fully metabolized by the RBCs to therefore yield a known amount of [3-^{13}C]L-lactate. A known amount of [6-^{13}C]L-methionine was also added to the sample, having confirmed that its resonance remained at the same intensity throughout many hours of incubation (more than 40 hours at 20°C or 24 hours at 37°C).

The concentration of [3-^{13}C]L-lactate was inferred from the ratio of its integral to that of [6-^{13}C]L-methionine. For a given NMR experiment with its specified relaxation delay(s), RF pulse angle(s), and acquisition time, a known concentration of lactate, C_1^{Cal}, gives a signal S_1^{Cal}

$$C_1^{Cal} = \varepsilon_1 S_1^{Cal} \tag{5}$$

where the subscript 1 denotes lactate ^{13}C-methyl, ε_1 is the "extinction coefficient" [mol liter^{-1} (unit of signal)$^{-1}$], and S_1^{Cal} is the numerical value of the signal. Similarly, for the standard [6-^{13}C]L-methionine (denoted by the subscript 2), we had

$$C_2^{Cal} = \varepsilon_2 S_2^{Cal} \tag{6}$$

The ratio of the two signals, $\frac{S_1^{Cal}}{S_2^{Cal}} = S_r^{Cal}$ (where r denotes ratio), is the most convenient way to record the data, so the ratio of the extinction coefficients, ε_r, becomes

$$\frac{\varepsilon_1}{\varepsilon_2} = \varepsilon_r = \frac{C_1^{Cal}}{C_2^{Cal} S_r^{Cal}} = \frac{C_r^{Cal}}{S_r^{Cal}} \tag{7}$$

Then, the calculated concentration of [3-^{13}C]L-lactate, C_1, in any ^{13}C NMR spectrum in the presence of a known concentration of [6-^{13}C]L-methionine, C_2, is given by

$$C_1 = \varepsilon_r S_r C_2 \tag{8}$$

This analysis was performed on the spectra shown in Fig. 2 and fig. S1 to calculate the effective glycolytic rates.

2) An alternative method to estimate the actual concentration of metabolites in RBC suspensions was to use the conservation of mass condition for ^{13}C-labeled species. A known amount of [1,6-^{13}C]D-glucose was added to the sample, typically 10 mM in 3 ml of RBC suspension, and at any time, all this "^{13}C-label" gave resonances effectively only from [1,6-^{13}C]D-glucose, [3-^{13}C]23BPG, or [1,3-^{13}C]L-lactate. Approximately 5% of the labeled metabolites were glycolytic and pentose-phosphate pathway intermediates that were in such low concentrations (*32*, *48*) that they were undetected in the ^{13}C NMR spectra (hence the word "effectively" above). Because progressive saturation affects the resonance intensity differently for each solute, it was necessary to calculate an effective extinction coefficient, ε_i (where i is the substrate label/abbreviation), that relates resonance intensity to concentration. This was solved using the conservation of mass (concentration) expression

$$\frac{1}{\varepsilon_{Glc}}\left(Sig_{GlcC1\beta} + Sig_{GlcC1\alpha} + Sig_{GlcC6\beta+\alpha} + Sig_{GlcC1\alpha}\right) + \frac{1}{\varepsilon_{BPG}} Sig_{BPG} + \frac{1}{\varepsilon_{Lact}} Sig_{Lact} = [Glc]_0 \tag{9}$$

where Sig_i denotes the resonance integral or amplitude (as appropriate), assuming equal extinction coefficients for different atoms and anomers of glucose.

The value of each $1/\varepsilon_i$ was estimated from all, or a subset, of the spectra in a time course such as that shown in Fig. 2 and fig. S1. Thus, the system of simultaneous algebraic equations was overdetermined and was therefore amenable to statistical analysis by using the function LinearModelFit in Mathematica (*49*). In addition, the concentration of [3-^{13}C]L-lactate was given by $\frac{1}{\varepsilon_{Lact}} Sig_{Lact}$ and so forth for the other species.

NMR spectroscopy

^{13}C NMR and ^{133}Cs NMR spectra were recorded at 100.61 and 52.48 MHz, respectively, on a Bruker Avance III spectrometer that has a 9.4-T vertical Oxford Instruments wide-bore magnet using a 10-mm broadband observe probe. Temperature was calibrated (Bruker script) using a sample of neat methanol; for gel-based experiments, it was set to 20°C to ensure persistence of the gel state, with its attendant elastic properties. A simple delay-pulse-acquire RF pulse sequence with CYCLOPS phase cycling was used to obtain the FIDs that were summed and then smoothed by exponential multiplication before Fourier transformation.

Computing

All spectra were phased and baseline-corrected in Bruker TopSpin 3.5 before they were imported into Mathematica (*49*) for postprocessing. The definitive metabolic experiments used [6-^{13}C]L-methionine as the internal intensity reference. Even for this compound, the calibration of peak intensities was necessary (see above) to account for progressive saturation in the rapid repetition spectral acquisition that was used to obtain the highest possible S/N ratio in a given time.

Progress curves of NMR spectral intensity were fitted by straight lines or exponential curves using the Mathematica (*49*) function

NonlinearModelFit; it returned estimates of intercept and slope of lines, and exponents in exponential curves, together with estimates of their SEs. When comparing two different slopes for a statistically significant difference, the standard two-tailed t test was used (*50*). Quantification of the septets obtained from $^{133}Cs^{+}$ in compressed gels was achieved by fitting, using NonlinearModelFit in Mathematica (*49*), the sum of seven Lorentzian functions of relative intensity 7:12:15:16:15:12:7 (*51*) to the spectra.

SUPPLEMENTARY MATERIALS

Supplementary material for this article is available at http://advances.sciencemag.org/cgi/content/full/3/10/eaao1016/DC1

Supplementary Discussion

Supplementary Methods

fig. S1. Control time course for the experiment in Fig. 1.

fig. S2. Efflux of Cs^{+} from human RBCs suspended in gelatin gel.

fig. S3. Influx of Cs^{+} to RBCs in gel-free suspension, in the presence of yoda1 at 37°C, measured with ^{133}Cs NMR spectroscopy.

table S1. Rates of [3-^{13}C]L-lactate production by human RBCs in the absence and presence of the Piezo1 activator yoda1 and several effector reagents.

References (*52*–*56*)

REFERENCES AND NOTES

1. S. Chien, Red cell deformability and its relevance to blood flow. *Annu. Rev. Physiol.* **49**, 177–192 (1987).
2. R. S. Sprague, E. A. Bowles, D. Achilleus, M. L. Ellsworth, Erythrocytes as controllers of perfusion distribution in the microvasculature of skeletal muscle. *Acta Physiol.* **202**, 285–292 (2011).
3. G. Pages, D. Szekely, P. W. Kuchel, Erythrocyte-shape evolution recorded with fast-measurement NMR diffusion–diffraction. *J. Magn. Reson. Imaging* **28**, 1409–1416 (2008).
4. P. W. Kuchel, E. D. Fackerell, Parametric-equation representation of biconcave erythrocytes. *Bull. Math. Biol.* **61**, 209–220 (1999).
5. R. I. Weed, P. L. LaCelle, E. W. Merrill, Metabolic dependence of red cell deformability. *J. Clin. Investig.* **48**, 795–809 (1969).
6. T. Browicz, Weitere beobachtungen uber bewegungsphanomene an roten blutkorperchen in pathologischen zustanden [Further observation of motion phenomena on red blood cells in pathological states]. *Zbl. Med. Wissen.* **28**, 625–627 (1890).
7. N. S. Gov, S. A. Safran, Red blood cell membrane fluctuations and shape controlled by ATP-induced cytoskeletal defects. *Biophys. J.* **88**, 1859–1874 (2005).
8. M. Puckeridge, P. W. Kuchel, Membrane flickering of the human erythrocyte: Constrained random walk used with Bayesian analysis. *Eur. Biophys. J.* **43**, 157–167 (2014).
9. M. Puckeridge, B. E. Chapman, A. D. Conigrave, P. W. Kuchel, Membrane flickering of the human erythrocyte: Physical and chemical effectors. *Eur. Biophys. J.* **43**, 169–177 (2014).
10. S. Tuvia, A. Almagor, A. Bitler, S. Levin, R. Korenstein, S. Yedgar, Cell membrane fluctuations are regulated by medium macroviscosity: Evidence for a metabolic driving force. *Proc. Natl. Acad. Sci. U.S.A.* **94**, 5045–5049 (1997).
11. T. Betz, M. Lenz, J.-F. Joanny, C. Sykes, ATP-dependent mechanics of red blood cells. *Proc. Natl. Acad. Sci. U.S.A.* **106**, 15320–15325 (2009).
12. J. Wan, A. M. Forsyth, H. A. Stone, Red blood cell dynamics: From cell deformation to ATP release. *Integr. Biol.* **3**, 972–981 (2011).
13. E. S. Haswell, R. Phillips, D. C. Rees, Mechanosensitive channels: What can they do and how do they do it? *Structure* **19**, 1356–1369 (2011).
14. B. Coste, J. Mathur, M. Schmidt, T. J. Earley, S. Ranade, M. J. Petrus, A. E. Dubin, A. Patapoutian, Piezo1 and Piezo2 are essential components of distinct mechanically activated cation channels. *Science* **330**, 55–60 (2010).
15. S. Sukharev, F. Sachs, Molecular force transduction by ion channels - Diversity and unifying principles. *J. Cell Sci.* **125**, 3075–3083 (2012).
16. B. Martinac, Mechanosensitive ion channels: An evolutionary and scientific tour de force in mechanobiology. *Channels* **6**, 211–213 (2012).
17. S. S. Ranade, R. Syeda, A. Patapoutian, Mechanically activated ion channels. *Neuron* **87**, 1162–1179 (2015).
18. P. G. Gillespie, R. G. Walker, Molecular basis of mechanosensory transduction. *Nature* **413**, 194–202 (2001).
19. F. Sachs, Mechanical transduction by ion channels: A cautionary tale. *World J. Neurol.* **5**, 74–87 (2015).
20. P. A. Gottlieb, C. Bae, F. Sachs, Gating the mechanical channel Piezo1: A comparison between whole-cell and patch recording. *Channels* **6**, 282–289 (2012).
21. C. Naumann, W. A. Bubb, B. E. Chapman, P. W. Kuchel, Tunable-alignment chiral system based on gelatin for NMR spectroscopy. *J. Am. Chem. Soc.* **129**, 5340–5341 (2007).
22. B. Luy, Distinction of enantiomers by NMR spectroscopy using chiral orienting media. *J. Indian Inst. Sci.* **90**, 119–132 (2010).
23. P. W. Kuchel, C. Naumann, $^{2}H_2O$ quadrupolar splitting used to measure water exchange in erythrocytes. *J. Magn. Reson.* **192**, 48–59 (2008).
24. P. W. Kuchel, D. Shishmarev, M. Puckeridge, M. H. Levitt, C. Naumann, B. E. Chapman, NMR of $^{133}Cs^{+}$ in stretched hydrogels: One-dimensional, z- and NOESY spectra, and probing the ion's environment in erythrocytes. *J. Magn. Reson.* **261**, 110–120 (2015).
25. D. Shishmarev, K. I. Momot, P. W. Kuchel, Anisotropic diffusion in stretched hydrogels containing erythrocytes: Evidence of cell-shape distortion recorded by PGSE NMR spectroscopy. *Magn. Reson. Chem.* **55**, 438–446 (2017).
26. R. Gnanasambandam, C. Bae, P. A. Gottlieb, F. Sachs, Ionic selectivity and permeation properties of human PIEZO1 channels. *PLOS ONE* **10**, e0125503 (2015).
27. T. Tiffert, J. L. Spivak, V. L. Lew, Magnitude of calcium influx required to induce dehydration of normal human red cells. *Biochim. Biophys. Acta* **943**, 157–165 (1988).
28. M. Puckeridge, B. E. Chapman, A. D. Conigrave, S. M. Grieve, G. A. Figtree, P. W. Kuchel, Stoichiometric relationship between Na^{+} ions transported and glucose consumed in human erythrocytes: Bayesian analysis of ^{23}Na and ^{13}C NMR time course data. *Biophys. J.* **104**, 1676–1684 (2013).
29. S. M. Cahalan, V. Lukacs, S. S. Ranade, S. Chien, M. Bandell, A. Patapoutian, Piezo1 links mechanical forces to red blood cell volume. *eLife* **4**, e07370 (2015).
30. P. W. Kuchel, Quadrupolar splittings in stretched hydrogels. *eMagRes* **3**, 171–180 (2014).
31. R. Syeda, J. Xu, A. E. Dubin, B. Coste, J. Mathur, T. Huynh, J. Matzen, J. Lao, D. C. Tully, I. H. Engels, H. M. Petrassi, A. M. Schumacher, M. Montal, M. Bandell, A. Patapoutian, Chemical activation of the mechanotransduction channel Piezo1. *eLife* **4**, e07369 (2015).
32. P. J. Mulquiney, P. W. Kuchel, *Modelling Metabolism with Mathematica* (CRC Press, 2003).
33. C. Gatto, M. A. Milanick, Inhibition of the red blood cell calcium pump by eosin and other fluorescein analogues. *Am. J. Physiol. Cell Physiol.* **264**, C1577–C1586 (1993).
34. G. Benga, B. E. Chapman, C. H. Gallagher, D. Cooper, P. W. Kuchel, NMR studies of diffusional water permeability of red blood cells from macropodid marsupials (kangaroos and wallabies). *Comp. Biochem. Physiol. Comp. Physiol.* **104**, 799–803 (1993).
35. C. L. Moore, Specific inhibition of mitochondrial Ca^{++} transport by ruthenium red. *Biochem. Biophys. Res. Commun.* **42**, 298–305 (1971).
36. S. Sasaki, M. Kanzaki, T. Kaneko, Calcium influx through TRP channels induced by short-lived reactive species in plasma-irradiated solution. *Sci. Rep.* **6**, 25728 (2016).
37. A. Athari, K. Jungermann, Unspecific inhibition by the calmodulin antagonist calmidazolium and the intracellular calcium antagonist TMB-8 of the actions of sympathetic hepatic nerves and noradrenaline on glucose balance and flow in perfused rat liver. *Biochem. Int.* **23**, 203–213 (1991).
38. T. M. Suchyna, J. H. Johnson, K. Hamer, J. F. Leykam, D. A. Gage, H. F. Clemo, C. M. Baumgarten, F. Sachs, Identification of a peptide toxin from *Grammostola spatulata* spider venom that blocks cation-selective stretch-activated channels. *J. Gen. Physiol.* **115**, 583–598 (2000).
39. C. Bae, F. Sachs, P. A. Gottlieb, The mechanosensitive ion channel Piezo1 is inhibited by the peptide GsMTx4. *Biochemistry* **50**, 6295–6300 (2011).
40. P. J. Mulquiney, W. A. Bubb, P. W. Kuchel, Model of 2,3-bisphosphoglycerate metabolism in the human erythrocyte based on detailed enzyme kinetic equations: In vivo kinetic characterization of 2,3-bisphosphoglycerate synthase/phosphatase using ^{13}C and ^{31}P NMR. *Biochem. J.* **342**, 567–580 (1999).
41. P. J. Mulquiney, P. W. Kuchel, Model of 2,3-bisphosphoglycerate metabolism in the human erythrocyte based on detailed enzyme kinetic equations: Equations and parameter refinement. *Biochem. J.* **342**, 581–596 (1999).
42. P. J. Mulquiney, P. W. Kuchel, Model of 2,3-bisphosphoglycerate metabolism in the human erythrocyte based on detailed enzyme kinetic equations: Computer simulation and metabolic control analysis. *Biochem. J.* **342**, 597–604 (1999).
43. T. Tiffert, R. M. Bookchin, V. L. Lew, Calcium homeostasis in normal and abnormal human red cells, in *Red Cell Membrane Transport in Health and Disease*, I. Bernhardt, J. C. Ellory, Eds. (Springer-Verlag, 2003).
44. A. J. Chang, F. E. Ortega, J. Riegler, D. V. Madison, M. A. Krasnow, Oxygen regulation of breathing through an olfactory receptor activated by lactate. *Nature* **527**, 240–244 (2015).
45. P. W. Kuchel, B. E. Chapman, N. Müller, W. A. Bubb, D. J. Philp, A. M. Torres, Apparatus for rapid adjustment of the degree of alignment of NMR samples in aqueous media: Verification with residual quadrupolar splittings in ^{23}Na and ^{133}Cs spectra. *J. Magn. Reson.* **180**, 256–265 (2006).
46. H. Cöulfen, W. Borchard, Determination of the partial specific volumes of thermoreversible gelatin/water and κ-carrageenan/water gels. *Macromol. Chem. Phys.* **195**, 1165–1175 (1994).

47. J. E. Raftos, B. T. Bulliman, P. W. Kuchel, Evaluation of an electrochemical model of erythrocyte pH buffering using ^{31}P nuclear magnetic resonance data. *J. Gen. Physiol.* **95**, 1183–1204 (1990).
48. E. Beutler, *Red Cell Metabolism: A Manual of Biochemical Methods* (Grune & Stratton, 1984).
49. S. Wolfram, *The Mathematica Book* (Wolfram Media Inc., ed. 5, 2003).
50. D. V. Huntsberger, *Elements of Statistical Inference* (Allyn & Bacon, 1961).
51. D. J. Philp, C. Naumann, P. W. Kuchel, Relative intensities of components of quadrupolar-split multiplets in NMR spectra: Rationale for a simple rule. *Concepts Magn. Reson.* **40A**, 90–99 (2012).
52. E. L. Watson, F. F. Vincenzi, P. W. Davis, Ca^{2+}-activated membrane ATPase: Selective inhibition by ruthenium red. *Biochim. Biophys. Acta* **249**, 606–610 (1971).
53. A. Lindner, E.-R. Gagne, J. Zingraff, P. Jungers, T. B. Drueke, P. Hannaert, R. Gara, A circulating inhibitor of the RBC membrane calcium pump in chronic renal failure. *Kidney Int.* **42**, 1328–1335 (1992).
54. K. W. Anderson, R. J. Coll, A. J. Murphy, Inhibition of skeletal muscle sarcoplasmic reticulum CaATPase activity by calmidazolium. *J. Biol. Chem.* **259**, 11487–11490 (1984).
55. B. Del Carlo, M. Pellegrini, M. Pellegrino, Calmodulin antagonists do not inhibit IK_{Ca} channels of human erythrocytes. *Biochim. Biophys. Acta* **1558**, 133–141 (2002).
56. G. Kummerlöwe, F. Halbach, B. Laufer, B. Luy, Precise measurement of RDCs in water and DMSO based gels using a silicone rubber tube for tunable stretching. *Open Spectroscopy J.* **2**, 29–33 (2008).

Acknowledgments: We thank C. Naumann for previous developments in stretched/compressed gel methodology for NMR spectroscopy, which were carried out in our laboratory; B. Martinac and C. Cox (Victor Chang Cardiac Research Institute, New South Wales) for valuable discussions on Piezo1; and A. Kwan for assistance with the maintenance of the NMR spectrometer. **Funding:** The work was supported by the Australian Research Council (grant DP140102596). **Author contributions:** P.W.K. conceived the experimental designs to study the reciprocity/duality of shape and energy consumption in RBCs. Both authors planned and jointly conducted all experiments and carried out the data analysis. P.W.K. drafted the manuscript and edited, with D.S., the final version. **Competing interests:** The authors declare that they have no competing interests. **Data and materials availability:** All data needed to evaluate the conclusions in the paper are present in the paper and/or the Supplementary Materials. Additional data related to this paper may be requested from the authors.

Submitted 14 June 2017
Accepted 21 September 2017
Published 18 October 2017
10.1126/sciadv.aao1016

Citation: P. W. Kuchel, D. Shishmarev, Accelerating metabolism and transmembrane cation flux by distorting red blood cells. *Sci. Adv.* **3**, eaao1016 (2017).

ScienceAdvances

Accelerating metabolism and transmembrane cation flux by distorting red blood cells

Philip W. Kuchel and Dmitry Shishmarev

Sci Adv **3** (10), eaao1016.
DOI: 10.1126/sciadv.aao1016